



# Impact of Footing Shape on Dynamic Properties and Vibration Transmission Characteristics of Machine Foundations

Sreyashrao Surapreddi<sup>1</sup> · Priyanka Ghosh<sup>1</sup>

Received: 16 June 2021 / Accepted: 5 December 2021 / Published online: 17 December 2021  
© The Author(s), under exclusive licence to Springer Nature Switzerland AG 2021

## Abstract

Due to immense infrastructure development activities, a study on the vibration generated by heavy machinery, construction activities, highway and railway traffic movements has gained importance in recent years. The present study investigates the influence of shape on the system and vibration transmission characteristics of block machine foundations under dynamic loading. A series of block vibration tests were conducted on model foundations laid on the local soil available at IIT Kanpur, India, to evaluate the system characteristics of machine foundations. The vibration transmission characteristics of the foundations were investigated using a 3D finite element (*FE*) analysis. Three different shapes of foundation (circular, square, and rectangular) were considered for the intended purpose. The effect of the loading intensity on various parameters such as natural frequency, soil stiffness, and damping coefficient was investigated. In addition, the shape effect of foundations on the dynamic shear strain, shear modulus, and the elastic uniform compression coefficient was suitably assessed. The efficiency of a wave barrier in mitigating the machine-induced vibration was investigated. It can be observed that the shape of foundations significantly influences the system characteristics. The circular and square foundations perform better than the rectangular foundation at higher loads. In contrast, the vibration transmission characteristics of block foundations are unaffected by the shape of the foundations. The transmission ratio decreases with an increase in the frequency at the pick-up points located away from the vibration source. It can be noted that the absolute damping varies significantly in the presence of the wave barrier at higher frequencies.

**Keywords** Machine foundation · Shape effect · Soil dynamics · Transmission ratio · Wave barrier

## Introduction

In recent times, due to rapid urbanization and scarcity of land, heavy machinery in several industrial projects affects the serviceability of nearby residential structures noticeably. The vibrations induced by such activities also cause discomfort to the residents and affect the functioning of different sophisticated instruments installed in the vicinity. Hence, a study on the vibration transmission characteristics under machine excitations is of paramount importance to understand the effect of induced vibration [1, 2]. The vibration characteristics of different machine foundations help us understand and subsequently design a structure as per the serviceability norms of the structure [3, 4]. Such

foundations may be of different shapes depending on the nature of the operating machinery. The shape of the foundation influences the dynamic properties of soil, such as approximate maximum dynamic shear strain developed in soil ( $\gamma_{res}$ ), shear modulus ( $G$ ), and elastic uniform compression coefficient ( $C_u$ ). The dynamic properties of soil vary significantly over a range of loading intensities in block vibration tests [5]. Hence, it is a gripping task to investigate the influence of footing shape on the system characteristics of machine foundations. The vibrations under the action of dynamic load produce both body and surface waves. Though the surface waves generally attenuate at a lesser rate than the body waves, their effect needs to be studied appropriately to mitigate the vibration-induced hazards [6]. The effect of such unwanted ground-borne vibration can be reduced by adopting various techniques such as modification of the attenuation characteristics of soil, application of wave barriers, or employment of damping devices in the form of base isolators [7–9]. Vibration mitigation using base isolators can

✉ Priyanka Ghosh  
priyog@iitk.ac.in

<sup>1</sup> Department of Civil Engineering, Indian Institute of Technology Kanpur, Kanpur 208 016, India

be an efficient alternative for mitigating earthquake-induced vibration. However, the implementation of such base isolators may turn out to be costly. If not implemented correctly, the soil characteristics near the structures may reduce the service span of the structures, which is undesirable [10]. Hence, in such cases, the wave barriers can be an ideal choice to avoid vibration-induced hazards [11]. The wave barriers can be implemented efficiently and economically in the form of open or in-filled trenches, which effectively mitigate the vibrations generated by various sources [12, 13]. Several researchers reported that the geometric properties of wave barriers and the dynamic properties of soil significantly affect the vibration screening performance [14].

Previous analytical studies [15, 16] and laboratory-scale model tests [17, 18] reported the effect of shape on the system characteristics of machine foundations. However, the impact of loading intensity on the vibration transmission characteristics of machine foundations has not drawn much attention from researchers. The present study explores the influence of foundation shape on the dynamic properties of soil through a series of field-scale block vibration tests with different geometries of block foundations. The dynamic properties of soil were evaluated by measuring the response near the source of vibration. The responses of different machine foundations were compared with the theoretical approaches to bolster the experimental findings further. To understand the shape effect, the evaluated dynamic properties for various foundations were compared. The vibration transmission characteristics of the block foundations were examined by conducting the three-dimensional finite element (*FE*) analysis in ABAQUS. By following the recommendation of Ghosh [19], a dynamic load was considered in the *FE* analysis to capture the vibration response of the soil. In addition, the effectiveness of wave barriers in mitigating machine-induced vibration was examined.

## Experimental Set-up

### Instrumentation

The vertical load was employed using a Lazan type mechanical oscillator, which consists of eight different positions of eccentric masses, as shown in Fig. 1. The angle between the eccentric masses can be varied to change the loading intensity. The oscillator employs the principle of the vector addition of two centrifugal forces to generate a resultant sinusoidal vibration. The specifications of the mechanical oscillator are described in Table 1. The magnitude of the vibrating force depends on the angular frequency and the eccentricity angle between the central and the extreme masses. Eccentricity may vary from  $0^\circ$  to  $180^\circ$ , and the force generated by the mechanical oscillator ( $F_o$ ) can be determined as



(a)



(b)

**Fig. 1** Cross-sectional view of mechanical oscillator: **a** eccentric masses and **b** shaft

**Table 1** Specifications of mechanical oscillator

Property	Value
Dynamic force (kgf)	2185
Eccentricity knobs	8
Output specification (HP)	3
Frequency range (Hz)	0–70

$$F_o = m_e \cdot e \cdot \omega^2 = \left(0.2684 \cos \frac{\theta}{2}\right) \omega^2 \quad (1)$$

where  $m_e$  is the unbalanced mass of the oscillator,  $e$  is the centre to centre distance between the shaft and the unbalanced masses,  $\omega$  is the operating angular frequency, and  $\theta$  is the angle between the eccentric masses. The tests were performed at three different eccentric mass settings such as

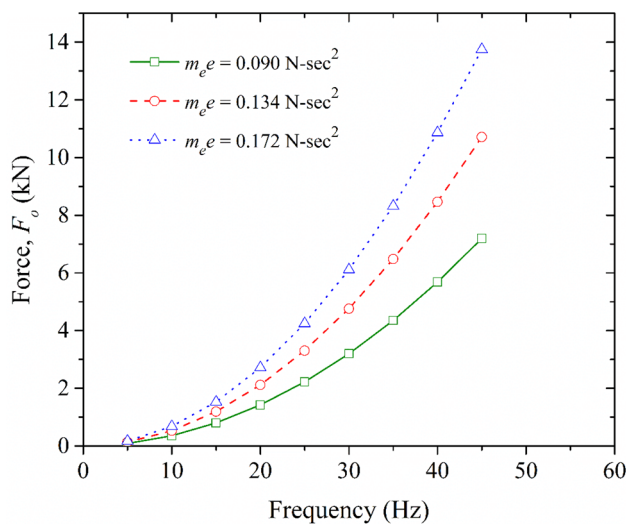


**Fig. 2** Force generated by mechanical oscillator at different eccentric force settings

**Table 2** Specifications of accelerometer

Parameter	Value
Model	603C02
Acceleration range (g)	± 10
Sensitivity (output) (mV/g)	550
Power supply (V)	5
Broadband resolution (µg)	300

100°, 120°, and 140°, generating the forces as 0.172 N-sec<sup>2</sup>, 0.134 N-sec<sup>2</sup>, and 0.09 N-sec<sup>2</sup>. It is worth mentioning that the eccentric angle denotes the angle between the central shaft and the extreme masses. Figure 2 depicts the force generated by the mechanical oscillator at various frequencies and different eccentric force settings.

In the present investigation, low g high output accelerometers were used, where g represents the acceleration due to gravity. Being an industrial piezoelectric sensor, the accelerometer measures the dynamic response of the system. It uses a piezoelectric sensing element to convert a mechanical phenomenon to an electrical signal. The specifications of the accelerometer are given in Table 2. The response data of the accelerometer was collected by a four-channel data acquisition system (DAQ). The DAQ consists of cables, measurement hardware, and a computer system with programmable software. The specifications of the DAQ used in the present study are given in Table 3. Vertical excitation was applied using the mechanical oscillator mounted on the foundation, as shown in the experimental set-up (Fig. 3). The oscillator was clamped to the foundation using a nut and bolt arrangement. The soil properties at the field location were adopted from Swain and Ghosh [20] and reported in

**Table 3** Specifications of DAQ system

Description	Value
Model	NI cDAQ-9171
Input FIFO size (samples)	127
Maximum sampling rate (samples/sec)	25,000
Timing accuracy (ppm)	50

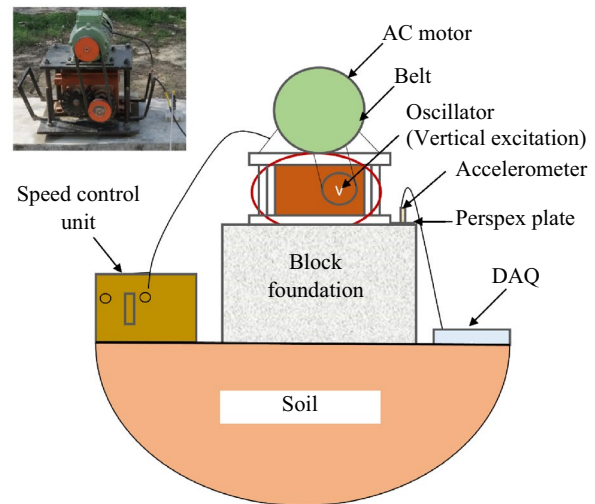


**Fig. 3** Experimental set-up with instrumentation

**Table 4** Index properties of soil after Swain and Ghosh [20]

Index property	Value
Liquid limit (%)	28.88
Plastic limit (%)	18.51
Plasticity index	10.37
Specific gravity	2.62
Sand fraction (%)	15.00
Silt fraction (%)	71.00
Clay fraction (%)	13.00
Optimum moisture content (%)	14.00
Maximum dry density (kg/m <sup>3</sup> )	1800
Poisson's ratio	0.30
Shear wave velocity (m/s)	225
Rayleigh wave velocity (m/s)	208
Rayleigh wavelength (λ <sub>R</sub> ) (m) at f=45 Hz	4.63
Modulus of elasticity (MPa)	237
Classification (USCS)	CL

Table 4. The soil can be characterized as low plasticity clay (CL) as per the Unified soil classification system (USCS) [21]. It is worth mentioning that a similar soil deposit was considered in the present study to evaluate the system characteristics of the machine foundation. By employing the

empirical correlations established between  $V_s$  and standard penetration test (SPT)  $N$  value, the shear wave velocities of the Kanpur local soil ( $V_s$ ) were estimated as 224.12 m/s and 224.68 m/s using Eqs. 2 and 3 [22, 23], respectively. Hence, the shear wave velocity was reasonably adopted as 225 m/s in the present study, as reported in Table 4.

$$V_s = 84.08N^{0.368} \quad (2)$$

$$V_s = 54.82N^{0.526} \quad (3)$$

## Reinforced Cement Concrete (RCC) Foundation

Block foundations with different shapes such as circular, rectangular, and square were employed in the experiment. A series of block vibration tests evaluated the system characteristics of the three types of foundations. Reinforced cement concrete (RCC) block foundations were made of M25 grade of concrete along with Fe 415 grade of reinforcement (12 mm diameter at 100 mm c/c). The width of the square foundation was taken as 0.75 m, whereas the length of the rectangular foundation was adopted as 1.05 m with an aspect ratio of 2.0. In contrast, the diameter of the circular foundation was considered as 0.85 m. However, the depth of all the foundations was kept as 0.45 m.

## Results and Discussion

### Block Vibration Tests

Block vibration tests were conducted on all the three foundations mentioned above. The force applied on the foundation is proportional to the applied frequency. The accelerometer was mounted on the top of the foundation to measure the response at the vibration source, as shown in Fig. 3. The acceleration was measured using LabView, followed by logical post-processing. It is worth mentioning that a MATLAB code was developed for post-processing, where the displacement- and velocity-time histories were obtained through the numerical integration of the acceleration time history. The steady-state peak displacements were noted. The response data collected for the circular, square, and rectangular foundations are shown in Fig. 4. It can be observed from Fig. 4 that with an increase in the magnitude of the eccentric force setting, the resonant amplitude increases, whereas the resonant frequency decreases.

The damping ratio,  $D$ , the natural frequency of the soil-foundation system  $f_n$ , the soil stiffness,  $k$  of the vibrating system, and the damping coefficient,  $c$ , were evaluated using Eqs. 4–7 [24].

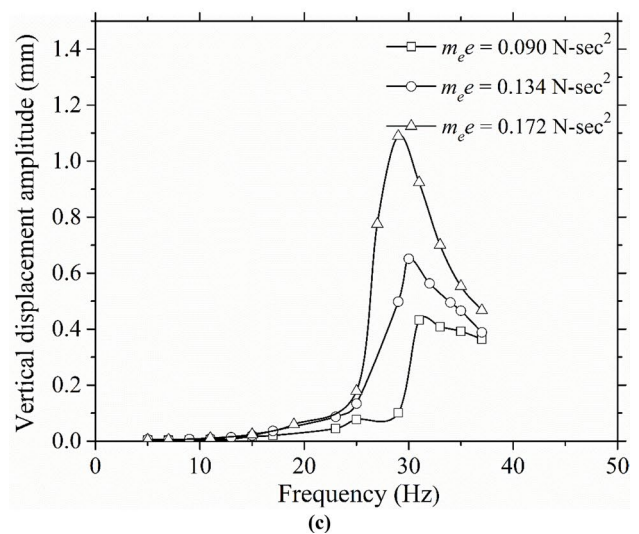
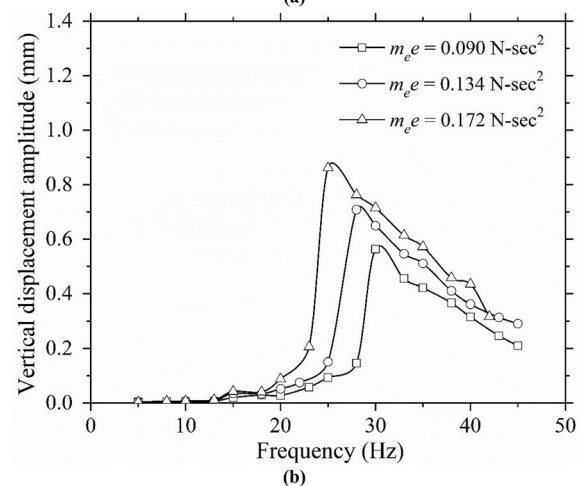
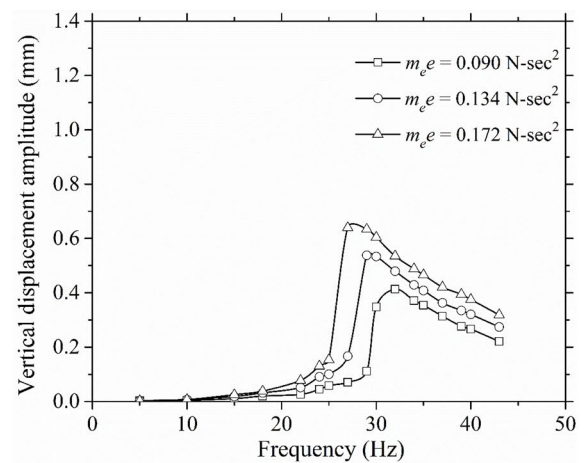


**Fig. 4** Variation of displacement amplitude with frequency for: **a** circular, **b** square and **c** rectangular foundations

$$\frac{z_r}{\frac{m_e e}{m}} = \frac{1}{2D\sqrt{1-D^2}} \tag{4}$$

$$f_n = f_{mr} \sqrt{1-2D^2} \tag{5}$$

$$k = m(2\pi f_n)^2 \tag{6}$$

$$c = 2D\sqrt{km} \tag{7}$$

where  $z_r$  is the peak vertical displacement of the system at resonance,  $m$  is the mass of the vibrating system, and  $f_{mr}$  is the resonant frequency of the soil-foundation system. The soil stiffness and the resonant frequency of the system decrease with an increase in the magnitude of the eccentric force setting irrespective of the shape of the foundation. The trends obtained from the present investigation are similar

**Table 5** Comparison of present results

Parameters	Swain and Ghosh [4]	Present study
Footing size (m)	0.55×0.55×0.20	0.75×0.75×0.45
Eccentric force (N-sec <sup>2</sup> )	0.017–0.033	0.090–0.172
Test results		
Resonant frequency (Hz)	37.21–32.93	30.00–25.00
Damping ratio (%)	16–18	10.28–12.89
Soil stiffness (MN/m)	16.92–13.76	27.17–18.63

to those observed by previous researchers [1, 4]. Since the applied force is proportional to the operating frequency, the natural frequency of the system is found to be lesser than the resonant frequency of the soil-foundation system. From Fig. 4b, the system characteristics for the square foundation were evaluated using Eqs. 4–7, and later, compared qualitatively with the results reported by Swain and Ghosh [4]

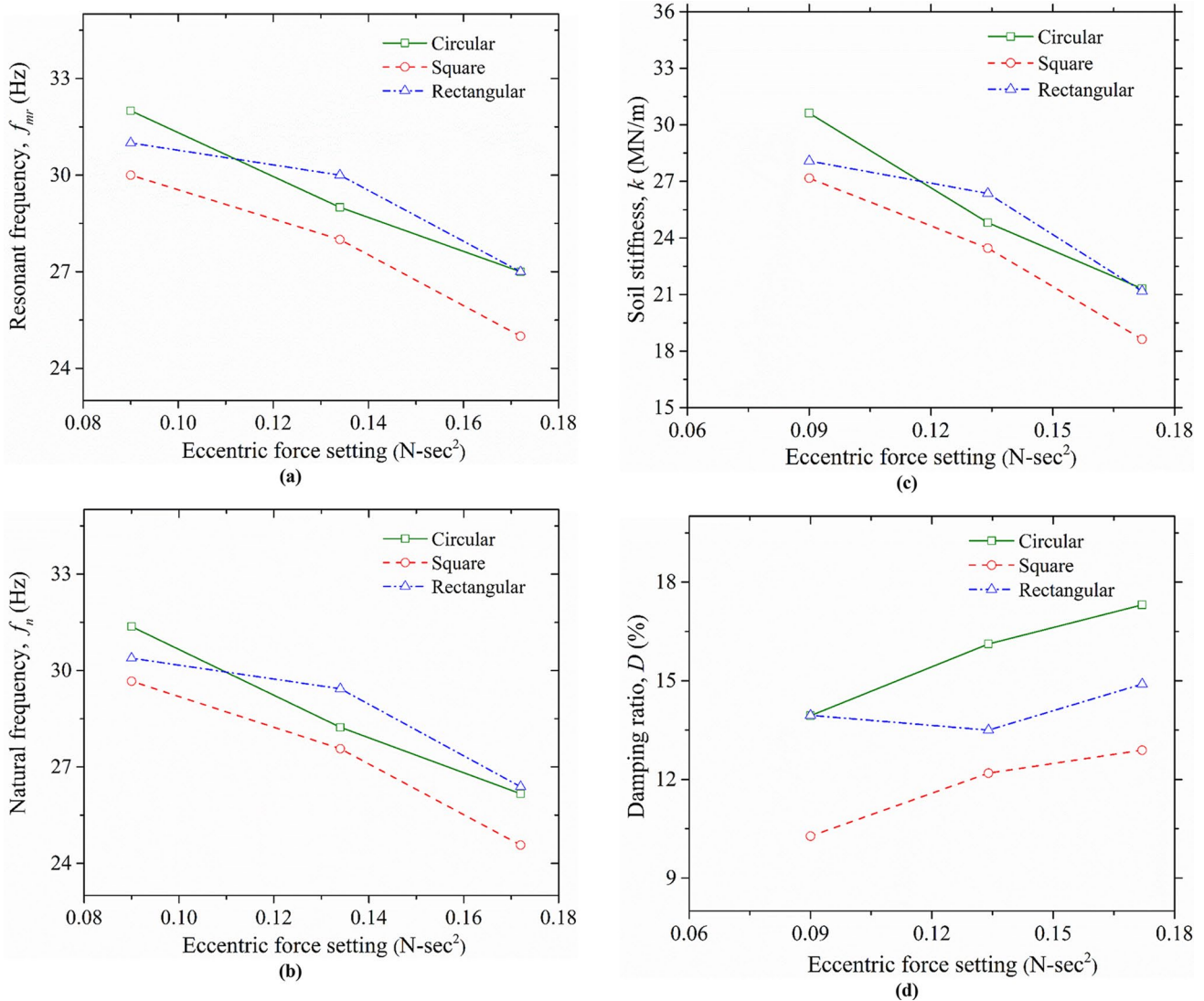


**Fig. 5** System characteristics of different foundations: **a** resonant frequency, **b** natural frequency, **c** soil stiffness, and **d** damping ratio

in Table 5. It is worth mentioning that Swain and Ghosh [4] also conducted block vibration tests on a similar soil deposit but with different foundation and loading conditions. It can be observed from Table 5 that with an increase in the magnitude of the eccentric force, the present value of the resonant frequency for the square foundation decreases from 30 to 25 Hz, but it decreases from 37.21 to 32.93 Hz in the study of Swain and Ghosh [4]. Such variation in the system characteristics may be attributed to the fact that the size of the foundation (0.75 m × 0.75 m × 0.45 m) and the magnitude of the eccentric force (0.09–0.172 N-sec<sup>2</sup>) considered in the present study are larger as compared to those adopted by Swain and Ghosh [4].

From Fig. 5a, it can be noted that the resonant frequency decreases from 32 to 27 Hz, 30–25 Hz, 31–27 Hz respectively for the circular, square, and rectangular foundations, with an increase in the eccentric force setting from 0.09 to 0.172 N-sec<sup>2</sup>. It can be seen from Fig. 5b that the natural frequency computed using Eq. 5 for the circular, square, and rectangular foundations decreases with an increase in the eccentric force setting. It can be observed from Fig. 5c that the stiffness of the soil decreases from 30.62 to 21.31 MN/m, 27.17–18.63 MN/m, 28.08–21.18 MN/m respectively for the circular, square, and rectangular foundations, with an increase in the value of the eccentric force setting from 0.09 to 0.172 N-sec<sup>2</sup>. In contrast, the damping ratio of the soil is found to increase from 13.94 to 17.31%, 10.28–12.89%, 13.94–14.90% for the circular, square, and rectangular foundations, respectively, as shown in Fig. 5d. To understand the variation in the system characteristics of the machine foundations, the dynamic properties of the soil ( $\gamma_{res}$ ,  $G$ , and  $C_u$ ) are investigated in detail in the subsequent sections.

### Dynamic Properties of Soil

The responses obtained from the block vibration tests were further utilized to evaluate the dynamic properties of soil ( $\gamma_{res}$ ,  $G$ , and  $C_u$ ). The magnitude of  $G$  varies perceptibly with the intensity of the applied force and the number of loading cycles [5], whereas  $C_u$  and  $\gamma_{res}$  vary continuously across the soil bed [25]. The magnitudes of  $\gamma_{res}$ ,  $G$ , and  $C_u$  were determined using Eqs. 8, 9, and 10 [5, 25, 26].

$$\gamma_{res} = \frac{z_r}{B} \tag{8}$$

$$G = \frac{1 - \mu}{4} \frac{k}{r} \tag{9}$$

$$C_u = \frac{4\pi^2 f_n^2 m}{A} \tag{10}$$

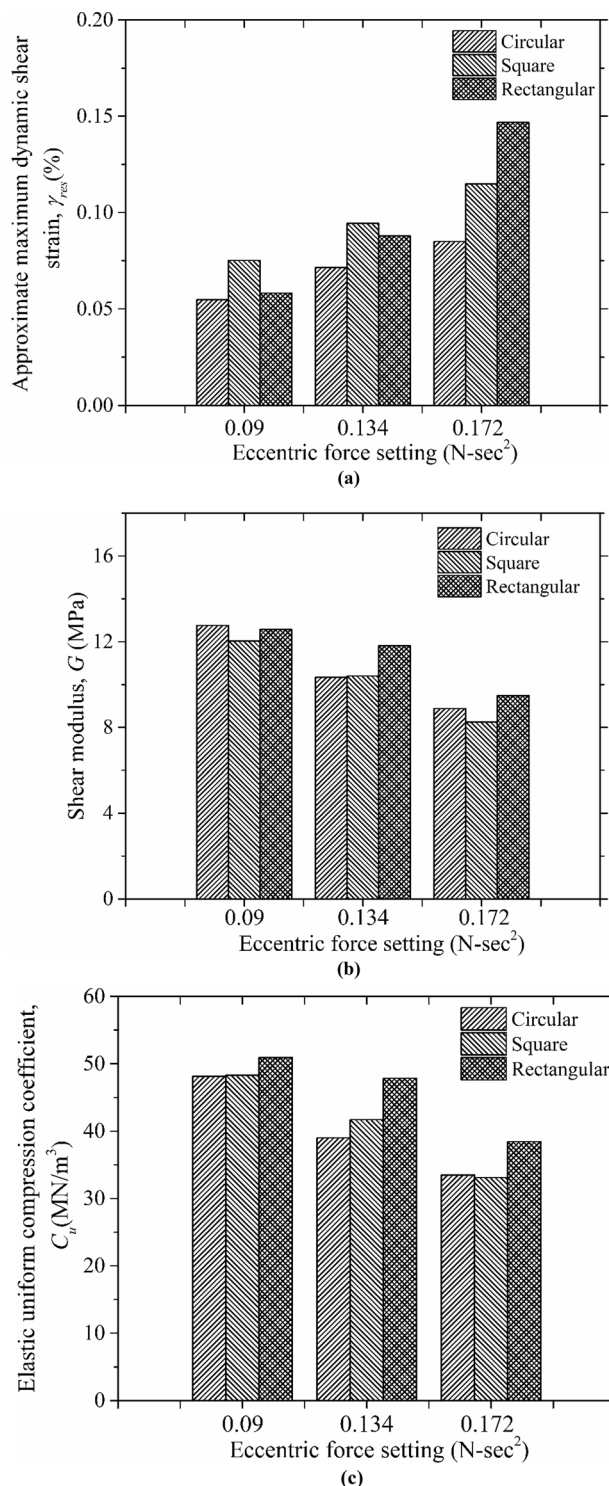


**Fig. 6** Comparison of dynamic properties: **a** approximate maximum dynamic shear strain, **b** shear modulus, and **c** elastic uniform compression coefficient

where  $\mu$  is the Poisson’s ratio of soil,  $r$  is the radius of the circular foundation or equivalent radius for the non-circular

foundation,  $A$  is the cross-sectional area of the block foundation, and  $B$  is the equivalent width of the foundation.

From Fig. 6a, it can be noted that the value of  $\gamma_{res}$  increases from 0.05 to 0.08%, 0.07–0.11%, 0.06–0.14% for the circular, square, and rectangular foundations, respectively with an increase in the eccentric force setting from 0.09 to 0.172 N-sec<sup>2</sup>. Kumar and Reddy [27] reported that the stiffness of the soil strata decreases with an increase in the dynamic shear strain in the soil. As observed earlier in Fig. 5c, the soil stiffness decreases by 30.40%, 31.42%, and 24.57% for the circular, square, and rectangular foundations, respectively, with an increase in the eccentric force setting from 0.09 to 0.172 N-sec<sup>2</sup>. Further, the shear modulus is influenced by the soil stiffness, as can be seen from Eq. 9. Hence, the shear modulus decreases with an increase in the applied force. From Fig. 6b, it can be noted that the value of  $G$  in the presence of the circular, square, and rectangular foundations decreases from 12.76 to 8.88 MPa, 12.04–8.25 MPa, 12.57–9.48 MPa, respectively, with an increase in the eccentric force setting from 0.09 to 0.172 N-sec<sup>2</sup>. The natural frequency of the system is proportional to the soil stiffness, as shown in Eq. 6. Figure 5b depicts that the natural frequency decreases by 15.63%, 16.67%, and 12.90% for the circular, square, and rectangular foundations, respectively, with an increase in the eccentric force setting 0.09–0.172 N-sec<sup>2</sup>. Since the mass and the area of the footings are constant, the natural frequency of the soil affects the elastic uniform compression coefficient significantly, as given in Eq. 10. The magnitude of  $C_u$  decreases from 48.13 to 33.51 MN/m<sup>3</sup>, 48.30–33.12 MN/m<sup>3</sup>, 50.94–38.42 MN/m<sup>3</sup> for the circular, square, and rectangular foundations, respectively, as shown in Fig. 6c.

### Analytical Solutions

In this study, the classical mass-spring-dashpot (MSD) system [1, 4, 28] and the modified elastic half-space theory (MEHST) [5, 26, 29] were considered to predict the response of the soil media analytically under different loading conditions. The soil stiffness ( $k$ ) and the damping coefficient ( $c$ ) of soil differ with varying loading intensities. The magnitudes of  $k$  and  $c$  were determined using Eqs. 6 and 7, respectively. However, the governing equation of motion for an idealized MSD system can be expressed as:

$$m \frac{d^2 z}{dt^2} + c \frac{dz}{dt} + kz = m_e e \omega^2 \sin(\omega t) \tag{11}$$

where  $\frac{d^2 z}{dt^2}$ ,  $\frac{dz}{dt}$  and  $z$  represent acceleration, velocity, and displacement, respectively. Hence, the displacement response of the MSD system can be determined from the following expression,

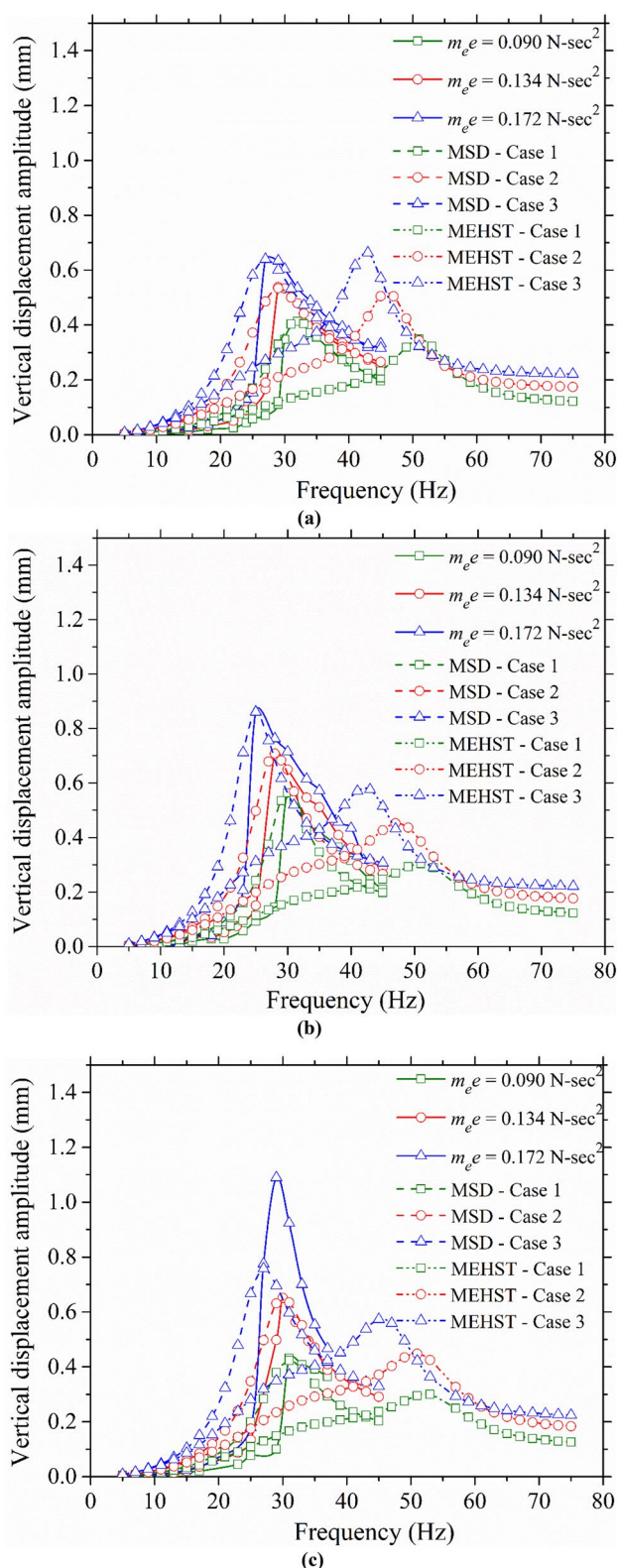


Fig. 7 Comparison of experimental results with analytical solutions: a circular, b square, and c rectangular foundations

$$z = \frac{\left(\frac{m_e e r_f^2}{m}\right)}{\sqrt{(1 - r_f^2)^2 + (2D r_f)^2}} \tag{12}$$

where  $r_f$  is the frequency ratio and is given by  $f/f_n$ .  $f$  is the input frequency of the mechanical oscillator. The magnitudes of  $D$  estimated from the field vibration tests were utilized to predict the response of the MSD analytical solution. As per the MEHST, the response of the system can be computed using Eqs. 13–17.

$$\frac{z_r}{\frac{m_e e}{m}} = B_z a_o^2 \left[ \frac{F_1^2 + F_2^2}{(1 - B_z a_o^2 F_1)^2 + (B_z a_o^2 F_2)^2} \right]^{1/2} \tag{13}$$

$$a_o = \frac{\omega r}{V_s} \tag{14}$$

$$B_z = \frac{(1 - \mu) m}{4 \rho r^3} \tag{15}$$

$$F_1 = 1.0 - 0.51741 a_o^2 + 0.10846 a_o^4 \tag{16}$$

$$F_2 = 0.5176 a_o - 0.26103 a_o^3 + 0.0383 a_o^5 \tag{17}$$

where  $a_o$  is the dimensionless frequency term,  $B_z$  is the modified mass ratio,  $\rho$  is the bulk density of the soil, and  $F_1$  and  $F_2$  are the modified displacement functions. The responses obtained from the MSD and the MEHST analytical solutions are compared with the experimental results in Fig. 7. It can be seen that the MSD analytical solution predicts the resonant frequency and the resonant amplitude favorably well. However, the MEHST analytical solution overestimates the resonant frequency and underestimates the resonant amplitude. Similar observations were also reported by Mandal et al. [5]. It can be seen from Fig. 7 that at the eccentric force setting of 0.172 N-sec<sup>2</sup>, the resonant frequency and amplitude obtained from the experiment for the rectangular foundation are higher compared to the response predicted by the analytical solution. In the case of the rectangular foundation, there may be eccentricity induced along the shorter span, which leads to a higher value of the displacement at the resonance. Hence, at higher loads, the response varies with the MSD analytical solution. It is worth noting that the responses of the circular and the square foundations compare reasonably well with the MSD analytical solution at the eccentric force setting of 0.172 N-sec<sup>2</sup>.

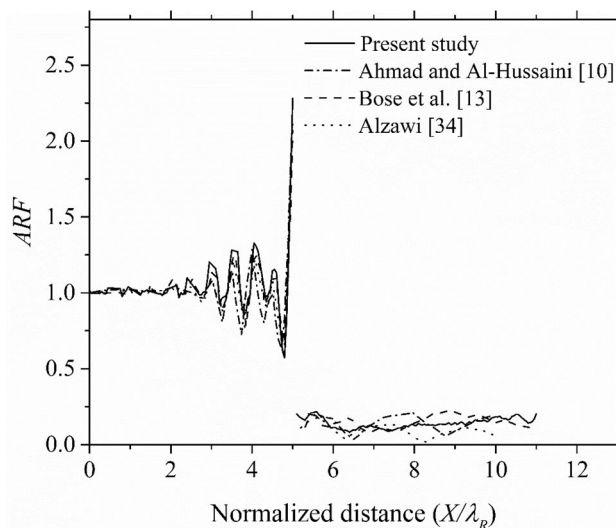


Fig. 8 FE model verification in the presence of wave barrier

### FE Modelling

In this section, the influence of shape on the vibration transmission characteristics of the block foundation was evaluated by performing a 3D FE analysis. The effectiveness of the wave barrier in mitigating vibrations was further investigated. The solid foundations were not considered for the analysis purpose, and the dynamic pressure was applied directly on the soil domain as it does not alter the study results [12, 13, 30]. The dimensions of the domain were normalized based on the Rayleigh wavelength ( $\lambda_R$ ) to ensure the accuracy of the analysis. Eight-noded first-order hexahedron elements were used for modelling the soil deposit. An average element size of 0.20 m was adopted, which satisfied the criteria recommended by Kramer [31] for a typical dynamic analysis. Non-reflecting semi-infinite boundaries (infinite elements) [32] were adopted in the domain using first-order eight-noded solid continuum elements as per the recommendations of Lysmer and Kuhlemeyer [33]. The input parameters such as density,  $\rho = 1800 \text{ kg/m}^3$ ; shear wave velocity,  $V_s = 101 \text{ m/s}$ ; Poisson’s ratio,  $\mu = 0.25$ ; and damping ratio,  $D = 5\%$  as reported by Ahmad and Al-Hussaini [10], Bose et al. [13], and Alzawi [34] were considered for the validation purpose. The wave barrier was placed at a distance of  $5\lambda_R$  from the source of excitation. The depth and the width of the wave barrier were taken as  $\lambda_R$  and  $0.06\lambda_R$ , respectively. A dynamic load of magnitude 1 kN and 31 Hz frequency was applied. The response was specified in terms of the amplitude reduction factor (ARF), where the ARF can be defined as,



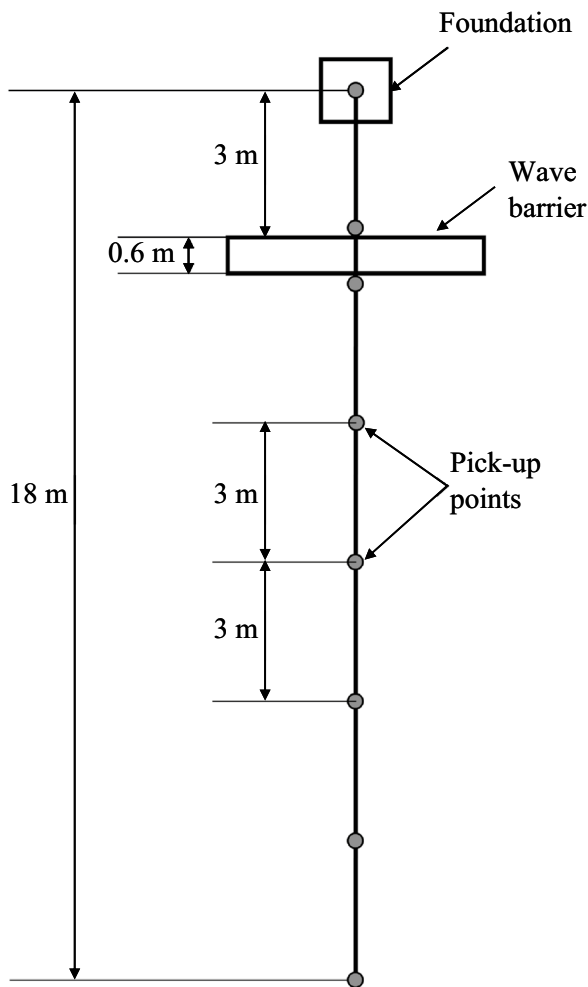


Fig. 9 Layout of pick-up points for the measurement of  $T_r$

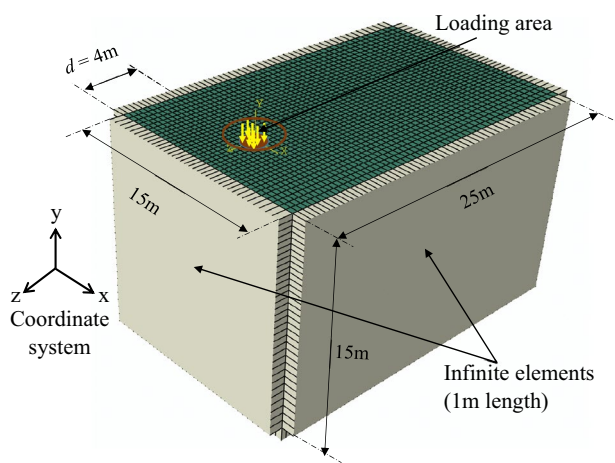


Fig. 10 Meshing scheme with infinite elements at the domain edges

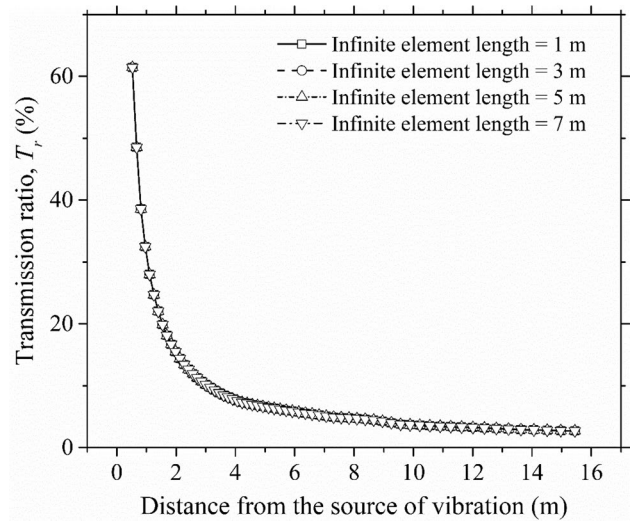


Fig. 11 Variation of transmission ratio with distance from the source of vibration for different lengths of infinite elements

$$ARF = \frac{(U_V)_{After}}{(U_V)_{Before}} \tag{18}$$

where  $(U_V)_{After}$  and  $(U_V)_{Before}$  are the steady-state peak vertical displacement amplitudes after and before installing the wave barrier, respectively. The present FE model favorably predicts the attenuation response of the wave barrier, as reported by Ahmad and Al-Hussaini [10], Bose et al. [13], and Alzawi [34] (Fig. 8). Hence, the present model can be utilized with confidence to investigate the attenuation response of the soil. Three different models were considered for the study to evaluate the transmission ratio, where the transmission ratio ( $T_r$ ) as per Eq. 19.

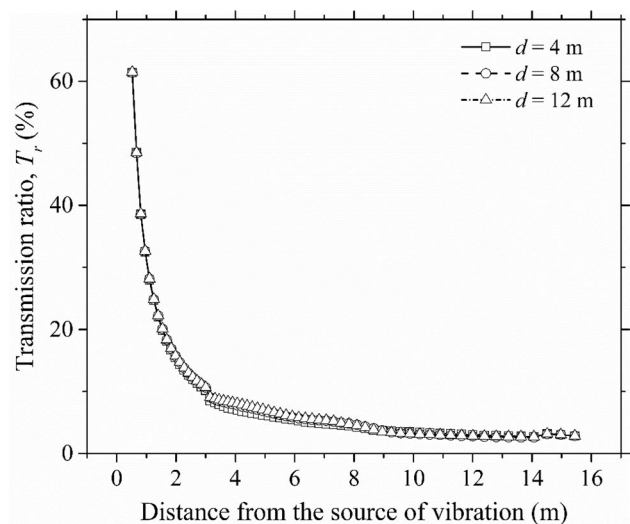
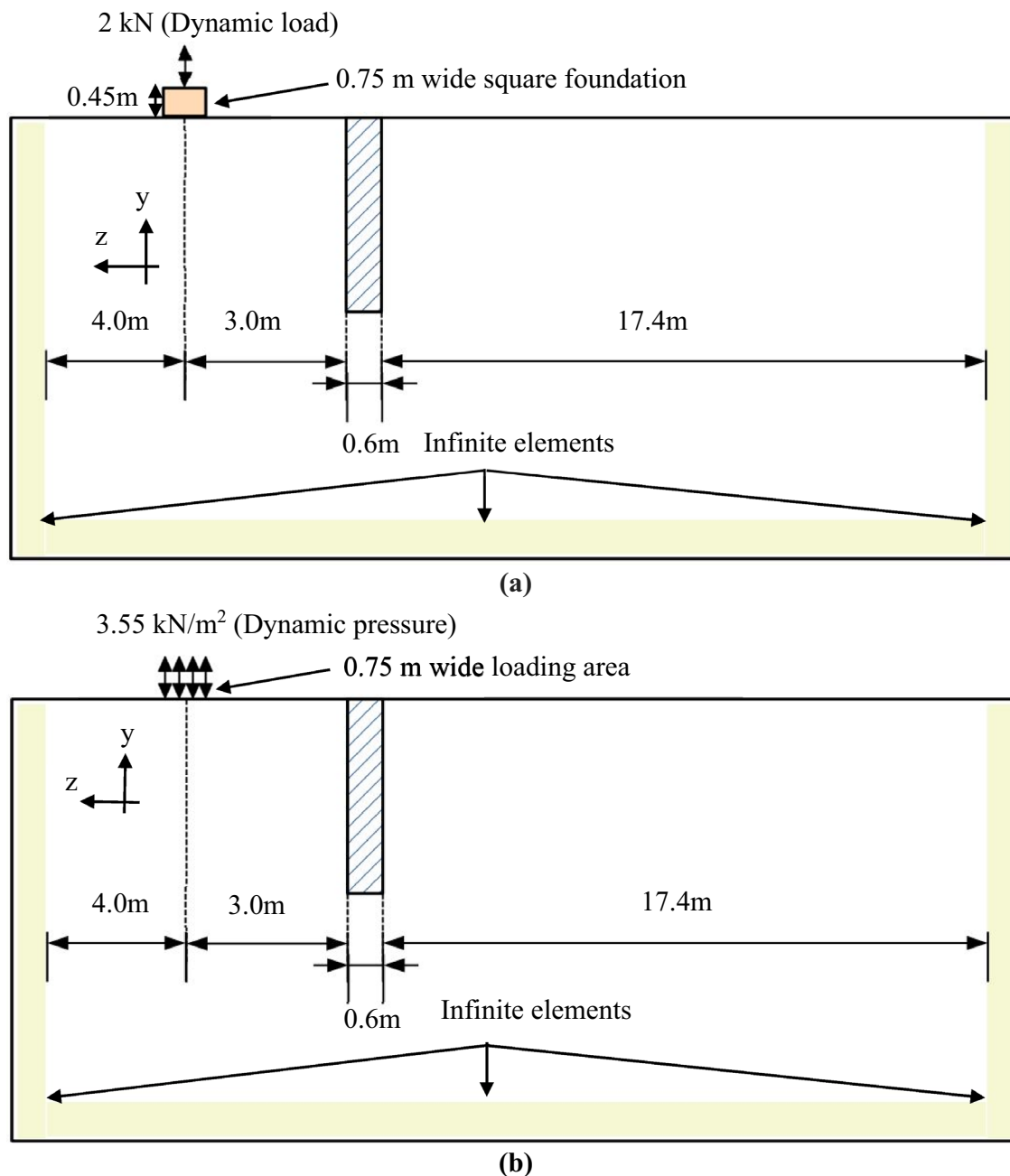


Fig. 12 Variation of transmission ratio with distance from the source of vibration for different values of  $d$  at a frequency of 30 Hz



**Fig. 13** Schematic for estimating the vibration transmission characteristics for the dynamic load applied directly on: **a** square foundation and **b** soil surface

$$T_r = \frac{\text{Vertical displacement amplitude at the pick-up point}}{\text{Vertical displacement amplitude at source}} \quad (19)$$

From the displacement-frequency response of the foundations (Fig. 4), it can be observed that the frequencies below 25 Hz do not get associated with significant amplitudes, and hence, they were ignored in this study.

Therefore, the frequencies adopted for the present study were in the range of 25–45 Hz. With a known frequency, the magnitude of  $\lambda_R$  can be obtained from the shear wave velocity profile of the soil [35]. The Rayleigh wavelength is found to decrease with an increase in frequency [6]. In this investigation,  $\lambda_R$  is found to be 4.63 m for the frequency of 45 Hz. Alzawi [34] and Mahdavisefat et al. [11] used a 3 m deep wave barrier in the experimental studies to evaluate the screening effectiveness of open and infilled

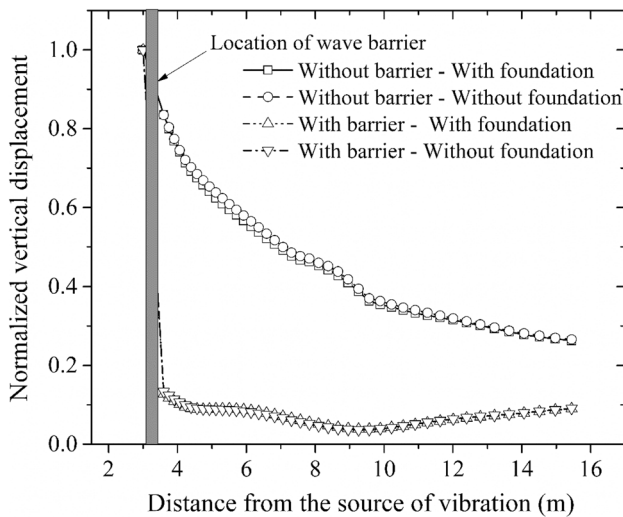


**Fig. 14** Variation of normalized vertical displacement with distance from the source of vibration with and without foundation

wave barriers. The normalized depth at a frequency of 45 Hz is found to be 0.64 for a 3-m deep wave barrier adopting the soil properties reported in Table 4. Woods [6] reported that wave barriers perform effectively at a normalized depth greater than 0.6. The normalized depth of the wave barrier considering a 3-m deep wave barrier satisfies the criteria recommended by Woods [6]. Further, the width and the length of the wave barrier do not influence the vibration transmission characteristics [6, 11, 34]. Hence, a wave barrier of 3 m depth, 0.6 m width, and 6 m length was reasonably adopted to study the reduction in the transmission ratio ( $T_r$ ), as depicted in Fig. 9. The response was captured at equally spaced pick-up points at an interval of 3 m, as shown in Fig. 9. Further, the effect of the wave barrier in impeding the vibrations generated at the source was also investigated. From the *FE* analysis, it was observed that the transmission ratio beyond 18 m is found to be around 2%. Additionally, the sensitivity analysis ensures that the amplitude of the waves becomes insignificant at the extreme boundaries ( $x$ - $z$  plane), which happens to be at a distance of 20 m from the source of vibration. The domain dimensions were accordingly chosen. Figure 10 depicts the domain dimensions and meshing scheme considered in the *FE* analysis.

Due to the wave propagation induced by dynamic loads, strains developed at the pick-up points located away from the vibration source are small in magnitude. The strain levels are further reduced in the presence of a wave barrier [13, 34, 36, 37]. Hence, for estimating the vibration transmission characteristics of the soil at different frequencies, the linear elastic constitutive model was reasonably adopted for the soil. Infinite elements [38, 39] were employed at the domain edges to prevent unwanted reflection of waves, as shown in

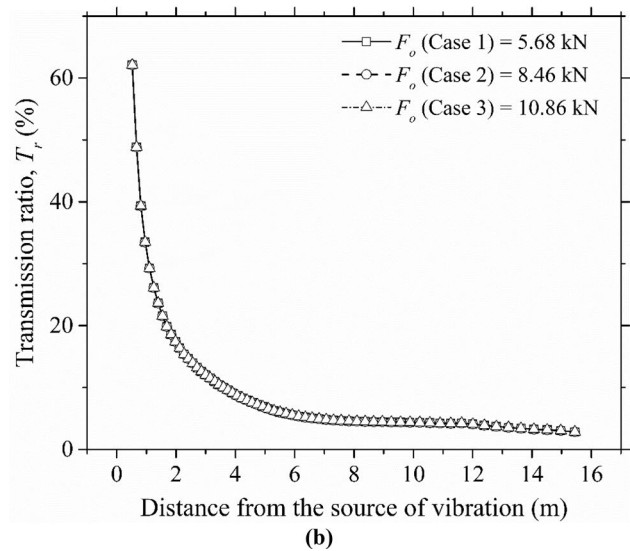
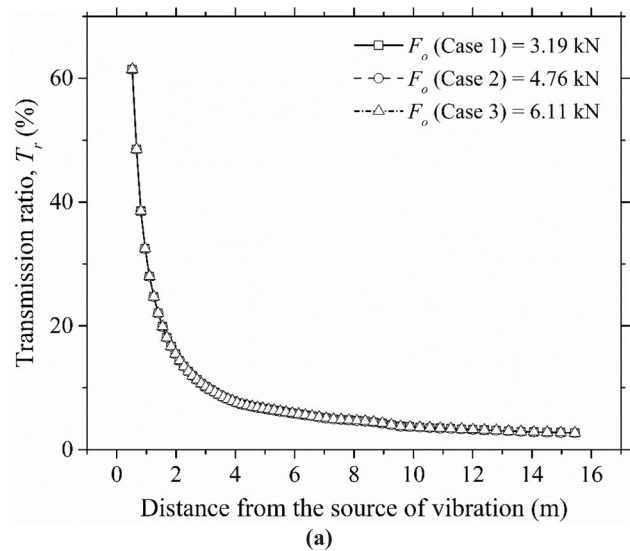


**Fig. 15** Transmission ratio for different loading configurations at frequencies: **a** 30 Hz and **b** 40 Hz

Fig. 10. The influence of the length of the infinite elements on the vibration transmission characteristics was investigated by performing a parametric study with different lengths of the infinite elements, such as 1 m, 3 m, 5 m, and 7 m. The material properties for the *FE* analysis were adopted from Table 4. The vibration transmission characteristics were evaluated at a frequency of 30 Hz and dynamic pressure of 2 kN/m<sup>2</sup>. From Fig. 11, it can be noted that the length of the infinite elements does not have a significant influence on the transmission ratio. Hence, in the present investigation, the infinite element length at the domain boundaries was adopted as 1 m. The influence of the distance ( $d$ ) between the domain edge and the source of vibration (Fig. 10) on the vibration transmission characteristics was also investigated through a parametric study considering  $d$  as 4 m, 8 m,

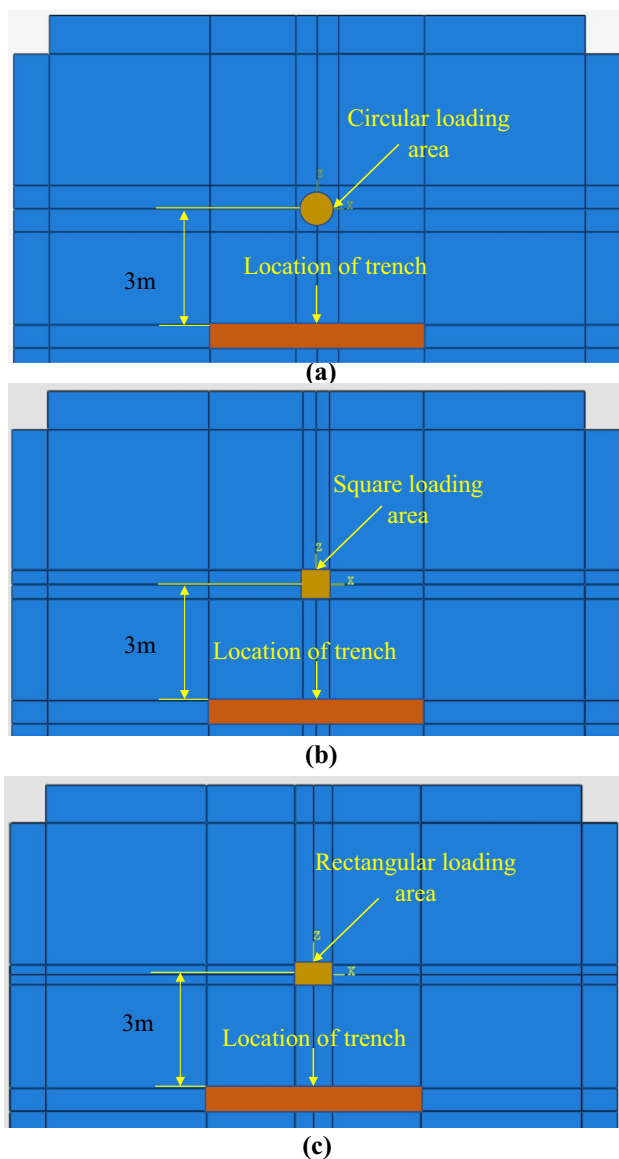


**Fig. 16** FE assembly showing the loading area for: **a** circular, **b** square and **c** rectangular foundations

and 12 m. It can be noticed from Fig. 12 that the vibration transmission characteristics compare favourably for different values of  $d$ . Hence,  $d$  was considered as 4 m to optimize the computational time for the *FE* analysis.

The normalized vertical displacement response was evaluated as per the schematic shown in Fig. 13 to investigate the influence of the actual foundation on the vibration transmission characteristics. It is worth noting that in Fig. 13a, the actual foundation exists, whereas the dynamic pressure is applied directly to the soil in Fig. 13b. A dynamic load of 2 kN was applied on top of the actual square foundation, as shown in Fig. 13a. The modulus of elasticity of the square foundation was taken as 25 GPa, whereas the density and the Poisson’s ratio were taken as 2500 kg/m<sup>3</sup> and 0.20, respectively [20]. A dynamic pressure of 3.55 kN/m<sup>2</sup> was applied over the area replicating the square foundation to evaluate the response without foundation, as shown in Fig. 13b. The responses were evaluated in the presence of the wave barrier. It can be conceived from Fig. 14 that the vibration transmission characteristics do not get affected in the presence and the absence of the solid foundation. Hence, solid footing was not adopted in the analysis to minimize the computational rigor [12, 13]. The effect of the dynamic load amplitudes corresponding to various eccentric force settings on the vibration transmission characteristics was explored. The dynamic loads at different eccentric force settings with 30 Hz and 40 Hz frequencies were considered, as shown in Fig. 2. Figure 15 shows that the dynamic load amplitudes do not affect the vibration transmission characteristics of the machine foundation significantly, where Case 1, Case 2, and Case 3 are the loads corresponding to the eccentric force settings of 0.090 N-sec<sup>2</sup>, 0.134 N-sec<sup>2</sup>, and 0.172 N-sec<sup>2</sup>, respectively. Similar observations were also reported by Bo et al. [40] and Mahdavisefat et al. [41]. Hence, for the present investigation, a dynamic pressure of 2 kN/m<sup>2</sup> was applied to the soil domain over an area replicating different geometries of the foundations. Thus, the *FE* model was adopted with confidence to study the influence

**Table 6** Transmission ratio for circular foundation with and without wave barrier

Distance (m) ↓	Transmission ratio $T_r$ (%)									
	Frequency (Hz) →									
	Without barrier					With barrier				
	25	30	35	40	45	25	30	35	40	45
3.0	10.23	10.28	10.75	12.41	11.80	30.27	25.59	23.82	24.24	24.22
3.6	8.74	8.59	8.90	10.32	10.10	5.54	3.41	3.90	5.38	5.97
6.0	5.60	5.96	5.74	5.72	5.43	3.52	2.15	1.32	1.27	1.40
9.0	4.06	4.29	4.55	4.58	4.11	2.21	0.96	0.93	0.87	0.92
12.0	3.31	3.28	3.34	4.20	3.77	2.50	1.64	1.23	1.02	0.78
15.0	2.95	2.77	2.68	3.11	2.89	3.00	2.24	1.46	0.84	0.52
18.0	3.21	2.98	2.53	2.20	1.93	2.94	2.35	1.49	1.11	1.08

**Table 7** Transmission ratio for square foundation with and without wave barrier

Distance (m) ↓	Transmission ratio $T_r$ (%)									
	Frequency (Hz) →									
	Without barrier					With barrier				
	25	30	35	40	45	25	30	35	40	45
3.0	10.12	10.16	10.64	12.04	11.57	29.96	25.31	23.53	23.51	23.79
3.6	8.65	8.48	8.81	10.01	9.90	5.51	3.38	3.86	5.24	5.92
6.0	5.54	5.89	5.67	5.56	5.34	3.49	2.13	1.31	1.24	1.39
9.0	4.01	4.25	4.50	4.44	4.03	2.19	0.95	0.92	0.85	0.91
12.0	3.27	3.25	3.31	4.09	3.71	2.48	1.62	1.22	0.99	0.78
15.0	2.92	2.74	2.65	3.03	2.86	2.98	2.21	1.45	0.82	0.51
18.0	3.18	2.94	2.50	2.13	1.89	2.92	2.33	1.48	1.08	1.07

**Table 8** Transmission ratio for rectangular foundation with and without wave barrier

Distance (m) ↓	Transmission ratio $T_r$ (%)									
	Frequency (Hz) →									
	Without barrier					With barrier				
	25	30	35	40	45	25	30	35	40	45
3.0	9.68	9.74	10.22	11.56	11.21	28.69	24.34	22.69	22.67	23.04
3.6	8.28	8.16	8.48	9.63	9.57	5.26	3.22	3.67	4.97	5.60
6.0	5.31	5.65	5.47	5.37	5.17	3.34	2.04	1.27	1.21	1.33
9.0	3.86	4.09	4.33	4.28	3.90	2.09	0.91	0.89	0.81	0.84
12.0	3.15	3.13	3.19	3.94	3.58	2.36	1.54	1.15	0.93	0.73
15.0	2.81	2.64	2.56	2.91	2.75	2.84	2.10	1.38	0.77	0.47
18.0	3.05	2.83	2.41	2.06	1.83	2.78	2.22	1.41	1.01	1.00

of different footing shapes on the vibration transmission characteristics of machine foundations. In the current *FE* analysis, the material properties were adopted from Table 4, and the damping ratio was reasonably assumed as 5% [13, 14]. Figure 16 shows different foundation shapes alongside the location of the wave barrier adopted in the *FE* analysis.

The transmission ratio ( $T_r$ ) at different pick-up points for all the foundations and the effect of the wave barrier are presented in Tables 6, 7, 8. It can be seen from Table 6 that with an increase in the frequency from 25 to 45 Hz, the transmission ratio for the circular foundation increases from 10.23 to 11.80% at the pick-up point located at 3 m from the source of vibration. However, in the presence of the wave barrier (Table 6), the reduction in  $T_r$  is found to be 36.65% and 40.86% at the frequencies 25–45 Hz, respectively. Similarly, Tables 7 and 8 show that at the pick-up point located at 3 m from the source of vibration, the transmission ratio for the square and the rectangular foundation increases from 10.12 to 11.57% and from 9.68 to 11.21%, respectively, with an increase in the frequency from 25 to 45 Hz. However, in the presence of the wave barrier (Tables 7 and 8), the reduction in  $T_r$  is seen to be 36.35% and 40.23% for the square

foundation, and 36.53% and 41.55% for the rectangular foundation at the frequencies 25–45 Hz, respectively. It can be conceived from Tables 6, 7, 8 that the values of  $T_r$  for all three foundations at various pick-up points compare well. It may be attributed to the fact that the geometric damping in the selected frequency range remains almost similar, and hence, the deviation is found to be marginal. Further, in the presence of the wave barrier, the reduction in  $T_r$  is found to be 8.39% and 44.05%, 8.25% and 43.69% and 8.92% and 45.37% for the circular, square, and rectangular foundations, respectively, at the frequencies 25 Hz and 45 Hz at 18 m from the source of vibration. Thus, at the pick-up points located away from the vibration source, the reduction in  $T_r$  is seen to be marginal at more minor frequencies. For the adopted parameters, the performance of the wave barrier turns out to be the best at a distance between 6 and 9 m from the vibration source. Such observations compare well with the results reported by Ahmad and Al-Hussaini [10] and Mahdavisefat et al. [11]. The impact of foundation shape on the vibration transmission characteristics can be further investigated by evaluating the absolute damping ( $D_a$ ) [42] at the pick-up points. The absolute damping can be expressed as

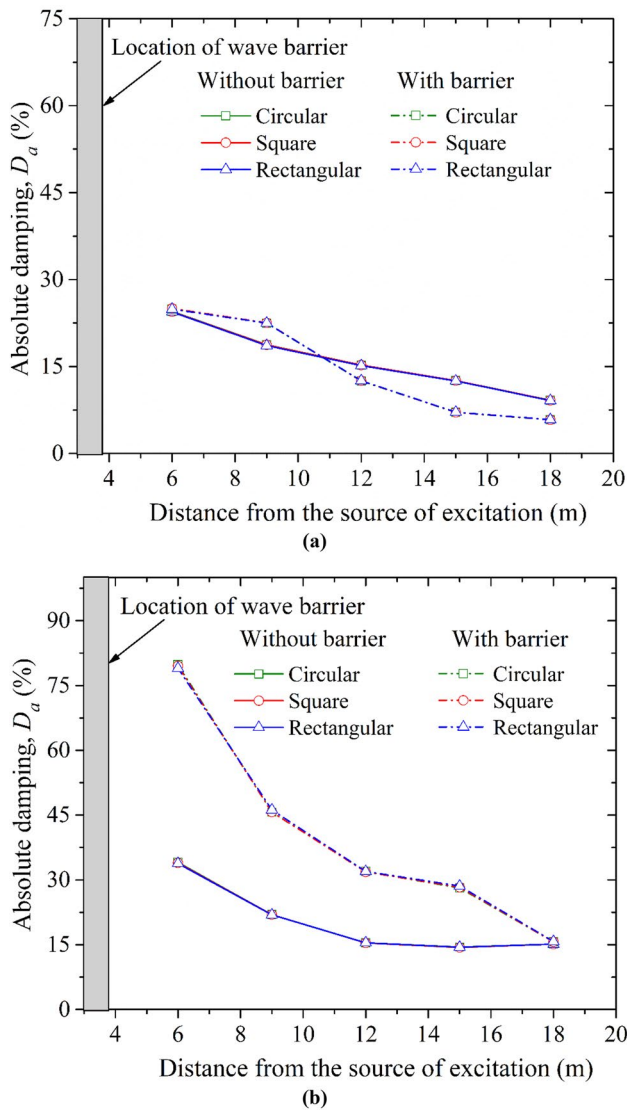


**Fig. 17** Variation of absolute damping with distance from the source of excitation at frequencies: **a** 25 Hz and **b** 45 Hz

$$D_a = \frac{V_R \ln\left(\frac{w_1}{w_2}\right)}{2\pi f \Delta x} \quad (20)$$

where  $V_R$  is the Rayleigh wave velocity, and  $\Delta x$  is the distance between the two measurements,  $w_{1,2}$  are the displacement amplitudes at different pick-up points located at a distance of  $r_{1,2}$  from the vibration source, and  $\ln\left(\frac{w_1}{w_2}\right)$  is the spectral ratio. The absolute damping computed at different pick-up points and the effect of wave barrier at different frequencies are presented in Fig. 17. As depicted in Fig. 17a, the absolute damping does not vary significantly in the presence of the wave barrier at a frequency of 25 Hz. In contrast, the absolute damping in the presence of the wave barrier increases significantly at a frequency of 45 Hz, as shown in

Fig. 17b. It can be revealed from Fig. 17 that in the presence of the wave barrier, the absolute damping at the pick-up point located at 6 m from the source of vibration increases from 24 to 34%, and from 24 to 79% at a frequency 25 Hz and 45 Hz, respectively. Hence, it is worth mentioning that the efficiency of wave barriers generally increases at higher frequencies. It can be seen from Fig. 17 that the magnitude of  $D_a$  for all three foundations does not vary much. Hence, it can be conceived that the shape of the foundation does not influence the vibration transmission characteristics much.

### Conclusions

Field-scale physical model tests were conducted on three different block foundations (circular, square, and rectangular), and the dynamic responses were studied at different load configurations. The dominant frequencies were identified, and the dynamic parameters were evaluated by performing block vibration tests. Further, the *FE* analysis was performed using ABAQUS to investigate the transmission ratio and the efficiency of the wave barrier in vibration mitigation. The major conclusions drawn from the study can be listed as:

- The dynamic shear strain increases from 0.05 to 0.08%, from 0.07 to 0.11%, and from 0.06 to 0.14% for the circular, square, and rectangular foundations, respectively, with an increase in the eccentric force setting from 0.09 to 0.172 N-sec<sup>2</sup>.
- The soil stiffness decreases by 30.40%, 31.42%, and 24.57% for the circular, square, and rectangular foundations, respectively, with an increase in the eccentric force setting from 0.09 to 0.172 N-sec<sup>2</sup>.
- The resonant frequency decreases by 15.63%, 16.67%, and 12.90% for the circular, square, and rectangular foundations, respectively, with an increase in the eccentric force setting from 0.09 to 0.172 N-sec<sup>2</sup>.
- At frequencies below 25 Hz, the displacement amplitudes are found to be negligible.
- The square and the circular foundations perform better than the rectangular foundation at higher dynamic loads. The resonant displacement amplitude tends to be more for the rectangular foundation at higher loads.
- The shape effect reasonably influences the system characteristics of the machine foundation, whereas the shape of the foundation does not affect the vibration transmission characteristics.
- For the adopted geometric configuration of the wave barrier, the best performance can be achieved at a distance of 6–9 m from the vibration source.
- The effectiveness of the wave barrier increases with an increase in frequency.

- In the presence of the wave barrier, the reduction in the transmission ratio at the pick-up point located at 18 m away from the source of vibration increases from 8 to 45%, with an increase in the frequency from 25 to 45 Hz.
- In the presence of the wave barrier, the absolute damping at the pick-up point located at 6 m away from the source of vibration increases from 24 to 34% and from 24 to 79% at frequencies 25 Hz and 45 Hz, respectively.

The present *FE* model can be suitably extended to other vibration-related problems such as railway and highway traffics, pile driving activities, and machines producing impact loads.

**Acknowledgements** The authors would like to acknowledge the financial support provided by the Council of Scientific and Industrial Research (CSIR), India, to carry out the present work through a sponsored research project (Ref No. 22(0731)/17/EMR-II).

**Author contributions** SS: methodology, experiment, formal analysis, investigation, validation, writing—original draft. PG: conceptualization, visualization, supervision, writing—review and editing.

**Data availability** Data sharing is not applicable to this article as no datasets were generated or analyzed during the current study.

## References

- Baidya DK, Krishna GM (2001) Investigation of resonant frequency and amplitude of vibrating footing resting on a layered soil system. *Geotech Test J* 24(4):409–417. <https://doi.org/10.1520/GTJ11138J>
- Venkateswarlu H, Sharma S, Hegde A (2021) Performance of genetic programming and multivariate adaptive regression spline models to predict vibration response of geocell reinforced soil bed: a comparative study. *Int J Geosynth Ground Eng* 7(3):1–17. <https://doi.org/10.1007/S40891-021-00306-6>
- Baidya DK, Krishna GM, Pradhan PK (2006) Investigation of foundation vibrations resting on a layered soil system. *J Geotech Geoenviron Eng* 132(1):116–123. [https://doi.org/10.1061/\(asce\)1090-0241\(2006\)132:1\(116\)](https://doi.org/10.1061/(asce)1090-0241(2006)132:1(116))
- Swain A, Ghosh P (2016) Experimental study on dynamic interference effect of two closely spaced machine foundations. *Can Geotech J* 53(2):196–209. <https://doi.org/10.1139/cgj-2014-0462>
- Mandal A, Baidya DK, Roy D (2012) Dynamic response of the foundations resting on a two-layered soil underlain by a rigid layer. *Geotech Geol Eng* 30(4):775–786. <https://doi.org/10.1007/s10706-012-9497-2>
- Woods RD (1968) Screening of surface wave in soils. *J Soil Mech Found Div* 94(4):951–979. <https://doi.org/10.1061/jsfeaq.0001180>
- Ngo NT, Indraratna B (2016) Improved performance of rail track substructure using synthetic inclusions: experimental and numerical investigations. *Int J Geosynth Ground Eng* 2(3):1–16. <https://doi.org/10.1007/s40891-016-0065-3>
- Moussa A, El Naggar H (2020) Numerical evaluation of buried wave barriers performance. *Int J Geosynth Ground Eng* 6(4):1–13. <https://doi.org/10.1007/s40891-020-00240-z>
- Wang J, Huang J (2021) Soil pressure reduction by including geofoam: a numerical study. *Int J Geosynth Ground Eng* 7(2):1–12. <https://doi.org/10.1007/S40891-021-00268-9>
- Ahmad S, Al-Hussaini TM (1991) Simplified design for vibration screening by open and in-filled trenches. *J Geotech Eng* 117(1):67–88. [https://doi.org/10.1061/\(ASCE\)0733-9410\(1991\)117:1\(67\)](https://doi.org/10.1061/(ASCE)0733-9410(1991)117:1(67))
- Mahdavisefat E, Salehzadeh H, Heshmati AA (2018) Full-scale experimental study on screening effectiveness of SRM-filled trench barriers. *Geotechnique* 68(10):869–882. <https://doi.org/10.1680/jgeot.17.P.007>
- Dasgupta B, Beskos DE, Vardoulakis IG (1990) Vibration isolation using open or filled trenches Part 2: 3-D homogeneous soil. *Comput Mech* 6(2):129–142. <https://doi.org/10.1007/BF00350518>
- Bose T, Choudhury D, Sprengel J, Ziegler M (2018) Efficiency of open and infill trenches in mitigating ground-borne vibrations. *J Geotech Geoenviron Eng* 144(8):1–11. [https://doi.org/10.1061/\(asce\)gt.1943-5606.0001915](https://doi.org/10.1061/(asce)gt.1943-5606.0001915)
- Majumder M, Ghosh P, Sathiyamoorthy R (2017) An innovative vibration barrier by intermittent geofoam-A numerical study. *Geomech Eng* 13(2):269–284. <https://doi.org/10.12989/gae.2017.13.2.269>
- Gazetas G, Dobry R, Tassoulas JL (1985) Vertical response of arbitrarily shaped embedded foundations. *J Geotech Eng* 111(6):750–771. [https://doi.org/10.1061/\(ASCE\)0733-9410\(1985\)111:6\(750\)](https://doi.org/10.1061/(ASCE)0733-9410(1985)111:6(750))
- Gazetas G (1991) Formulas and charts for impedances of surface and embedded foundations. *J Geotech Eng* 117(9):1363–1381. [https://doi.org/10.1061/\(ASCE\)0733-9410\(1991\)117:9\(1363\)](https://doi.org/10.1061/(ASCE)0733-9410(1991)117:9(1363))
- Dobry R, Gazetas G (1986) Dynamic response of arbitrarily shaped foundations. *J Geotech Eng* 112(2):109–135. [https://doi.org/10.1061/\(ASCE\)0733-9410\(1986\)112:2\(109\)](https://doi.org/10.1061/(ASCE)0733-9410(1986)112:2(109))
- Gazetas G, Stokoe KH (1991) Free vibration of embedded foundations: theory versus experiment. *J Geotech Eng* 117(9):1382–1401. [https://doi.org/10.1061/\(ASCE\)0733-9410\(1991\)117:9\(1382\)](https://doi.org/10.1061/(ASCE)0733-9410(1991)117:9(1382))
- Ghosh P (2012) FLAC based numerical studies on dynamic interference of two nearby embedded machine foundations. *Geotech Geol Eng* 30(5):1161–1181. <https://doi.org/10.1007/s10706-012-9530-5>
- Swain A, Ghosh P (2019) Determination of viscoelastic properties of soil and prediction of static and dynamic response. *Int J Geomech* 19(7):04019072. [https://doi.org/10.1061/\(asce\)gm.1943-5622.0001456](https://doi.org/10.1061/(asce)gm.1943-5622.0001456)
- ASTM D2487-17e1 Standard practice for classification of soils for engineering purposes (Unified soil classification system). ASTM International, USA
- Naik SP, Patra NR, Malik JN (2014) Spatial distribution of shear wave velocity for late quaternary alluvial soil of Kanpur city Northern India. *Geotech Geol Eng* 32(1):131–149. <https://doi.org/10.1007/s10706-013-9698-3>
- Chatterjee K, Choudhury D (2013) Variations in shear wave velocity and soil site class in Kolkata city using regression and sensitivity analysis. *Nat Hazards* 69(3):2057–2082. <https://doi.org/10.1007/s11069-013-0795-7>
- Lysmer J, Richart FE (1966) Dynamic response of footings to vertical loading. *J Soil Mech Found Div* 92(1):65–91. <https://doi.org/10.1061/jsfeaq.0000846>
- Prakash S, Puri VK (1981) Dynamic properties of soils from in-situ tests (India). *J Geotech Eng* 107(7):943–963. <https://doi.org/10.1061/AJGEB6.0001171>
- Zakeri R, Tafreshi SN, Dawson AR, Baidya DK (2021) Influence of rubber sheet on dynamic response of machine foundations. *Constr Build Mater* 274:121788. <https://doi.org/10.1016/j.conbuildmat.2020.121788>

27. Kumar J, Reddy CO (2006) Dynamic response of footing and machine with spring mounting base. *Geotech Geol Eng* 24(1):15–27. <https://doi.org/10.1007/s10706-004-1806-y>
28. Venkateswarlu H, Hegde A (2020) Effect of influencing parameters on the vibration isolation efficacy of geocell reinforced soil beds. *Int J Geosynth Ground Eng* 6:1–17. <https://doi.org/10.1007/s40891-020-00205-2>
29. Richart FE Jr, Hall JR, Woods RD (1970) *Vibrations of soils and foundations*. Prentice-Hall, Inc., Englewood Cliffs
30. Surapreddi S, Ghosh P (2021) Experimental and numerical investigations on attenuation response of machine foundations under vertical excitation. *Geomech Geoengin*. <https://doi.org/10.1080/17486025.2021.1980231>
31. Kramer SL (1996) *Geotechnical earthquake engineering*. Prentice-Hall, New Jersey
32. Nanda RP, Dutta S, Das A, Khan HA (2017) Geosynthetic liner as foundation isolation for seismic protection. *Int J Geosynth Ground Eng* 3(3):1–7. <https://doi.org/10.1007/S40891-017-0098-2>
33. Lysmer J, Kuhlemeyer RL (1969) Finite dynamic model for infinite media. *J Eng Mech Div* 95(4):859–877. <https://doi.org/10.1061/jmcea3.0001144>
34. Alzawi A (2011) *Vibration isolation using in-filled geofoam trench barriers*. Dissertation, The University of Western Ontario. <https://ir.lib.uwo.ca/etd/265>. Accessed 3 Apr 2021
35. Kirar B, Maheshwari BK, Muley P (2016) Correlation between shear wave velocity ( $V_s$ ) and SPT resistance ( $N$ ) for Roorkee region. *Int J Geosynth Ground Eng* 2(1):9. <https://doi.org/10.1007/s40891-016-0047-5>
36. Yang YB, Hung HH (1997) A parametric study of wave barriers for reduction of train-induced vibrations. *Int J Numer Methods Eng* 40(20):3729–3747. [https://doi.org/10.1002/\(SICI\)1097-0207\(19971030\)40:20%3c3729::AID-NME236%3e3.0.CO;2-8](https://doi.org/10.1002/(SICI)1097-0207(19971030)40:20%3c3729::AID-NME236%3e3.0.CO;2-8)
37. Andersen L, Nielsen SRK (2005) Reduction of ground vibration by means of barriers or soil improvement along a railway track. *Soil Dyn Earthq Eng* 25(7–10):701–716. <https://doi.org/10.1016/j.soildyn.2005.04.007>
38. Khan MR, Dasaka SM (2020) Amplification of vibrations in high-speed railway embankments by passive ground vibration barriers. *Int J Geosynth Ground Eng* 6(3):1–15. <https://doi.org/10.1007/s40891-020-00217-y>
39. Khan MR, Dasaka SM (2020) EPS geofoam as a wave barrier for attenuating high-speed train-induced ground vibrations: a single-wheel analysis. *Int J Geosynth Ground Eng* 6(4):1–13. <https://doi.org/10.1007/s40891-020-00230-1>
40. Bo Q, Ali L, Irini DM (2014) Numerical study of wave barrier and its optimization design. *Finite Elem Anal Des* 84:1–13. <https://doi.org/10.1016/J.FINEL.2014.02.002>
41. Mahdavisefat E, Heshmati A, Salehzadeh H, Bahmani H, Sabermahani M (2017) Vibration screening by trench barriers, a review. *Arab J Geosci* 10(23):1–14. <https://doi.org/10.1007/s12517-017-3279-3>
42. Zerwer A, Cascante G, Hutchinson J (2002) Parameter estimation in finite element simulations of Rayleigh waves. *J Geotech Geoenviron Eng* 128(3):250–261. [https://doi.org/10.1061/\(asce\)1090-0241\(2002\)128:3\(250\)](https://doi.org/10.1061/(asce)1090-0241(2002)128:3(250))

**Publisher's Note** Springer Nature remains neutral with regard to jurisdictional claims in published maps and institutional affiliations.